THE JOURNAL OF PHYSICAL CHEMISTRY C

Subscriber access provided by OAK RIDGE NATIONAL LAB

C: Plasmonics; Optical, Magnetic, and Hybrid Materials

Ultrafast Exciton Dissociation at the 2D-WS Monolayer/Perovskite Interface

Joshua Bauer, Leo Scott Quintanar, Kai Wang, Alexander A. Puretzky, Kai Xiao, David B. Geohegan, and Abdelaziz Boulesbaa

J. Phys. Chem. C, **Just Accepted Manuscript** • DOI: 10.1021/acs.jpcc.8b08183 • Publication Date (Web): 29 Nov 2018

Downloaded from http://pubs.acs.org on December 4, 2018

Just Accepted

"Just Accepted" manuscripts have been peer-reviewed and accepted for publication. They are posted online prior to technical editing, formatting for publication and author proofing. The American Chemical Society provides "Just Accepted" as a service to the research community to expedite the dissemination of scientific material as soon as possible after acceptance. "Just Accepted" manuscripts appear in full in PDF format accompanied by an HTML abstract. "Just Accepted" manuscripts have been fully peer reviewed, but should not be considered the official version of record. They are citable by the Digital Object Identifier (DOI®). "Just Accepted" is an optional service offered to authors. Therefore, the "Just Accepted" Web site may not include all articles that will be published in the journal. After a manuscript is technically edited and formatted, it will be removed from the "Just Accepted" Web site and published as an ASAP article. Note that technical editing may introduce minor changes to the manuscript text and/or graphics which could affect content, and all legal disclaimers and ethical guidelines that apply to the journal pertain. ACS cannot be held responsible for errors or consequences arising from the use of information contained in these "Just Accepted" manuscripts.

ACS Publications

is published by the American Chemical Society. 1155 Sixteenth Street N.W., Washington, DC 20036

Published by American Chemical Society. Copyright © American Chemical Society. However, no copyright claim is made to original U.S. Government works, or works produced by employees of any Commonwealth realm Crown government in the course of their duties.

Ultrafast Exciton Dissociation at the 2D-Ws_2 Monolayer/Perovskite Interface

Joshua Bauer[a,#], Leo Scott Quintanar[a,#], Kai Wang[b], Alexander A. Puretzky[b], Kai Xiao[b], David B. Geohegan[b], and Abdelaziz Boulesbaa[a,*]

[a] Department of Chemistry & Biochemistry, California State University, Northridge, 18111 Nordhoff Street, Northridge, 91330 CA, USA

[b] Center for Nanophase Materials Sciences, Oak Ridge National Laboratory, 1 Bethel Valley Road, Oak Ridge, 37831 TN, USA

[#]Contributed equally

*Address correspondence to aboules@csun.edu

Abstract: In order for an excitonic photovoltaic (PV) device to perform efficiently, photogenerated excitons in the charge donor need to be dissociated through charge transfer (CT) to the acceptor rapidly after their photogeneration, and remain separated for a longer time to allow the collection of charges. To improve the efficiency of these steps, several combination of materials have been examined. Due to their excellent optical properties, two-dimensional transition metal dichalcogenides (2D-TMDs) have recently been explored. Another promising class of materials to platform efficient PVs is organic-inorganic perovskites. Here, we report on the ultrafast exciton dissociation through electron transfer from a 2D tungsten disulfide (WS_2) monolayer to a thin layer of methylammonium lead iodide ($CH_3NH_3PbI_3$) perovskites. Photoluminescence (PL) measurements showed that when the 2D-WS_2 monolayer was covered with perovskites, its emission completely quenched, suggesting that the CT process is highly efficient. Despite that pump-probe spectroscopy measurements were carried out with a ~ 45 fs

temporal resolution, the CT dynamics were not captured. A comparison of the ultrafast dynamics of the two band-edge excitons of the charge donor (2D-WS_2) suggested that electron transfer is the dominant pathway of CT. Furthermore, these pump-probe measurements indicated that a small fraction of transferred electrons remained in the perovskites up to almost 2 ns. These findings may open a new horizon for understanding the dissociation of photogenerated excitons in 2D-TMD through hybridization with other class of nanomaterials.

INTRODUCTION

Understanding the process of converting solar light into electricity has been a focus of several research fields, including photophysics, photochemistry, and material sciences. One indispensable step during the conversion process is charge transfer (CT). For instance, in order for an excitonic solar cell (SC) to operate efficiently, the charge donor has to have a high absorption cross section over a broad range within the solar spectrum, and the photogenerated excitons need to efficiently dissociate through CT to the acceptor[1-3]. Lately, a few attempts incorporated two-dimensional transition metal dichalcogenides (2D-TMDs) in SCs and demonstrated disappointing conversion efficiencies[4-6]. Even though these materials absorb light up to 10% within the solar spectrum[6], and have excitons with long diffusion lengths[7-9], up to 150 nm in the case of tungsten diselenide (WSe_2) monolayer[9], 2D-TMD based SCs demonstrated disappointing conversion efficiencies[4-6]. One possible reason for this discouraging conversion efficiency is that excitons in these materials are tightly bound[10-11], which makes their dissociation challenging. However, in hybrid organic-inorganic perovskites family of materials ABX_3 ($A=CH_3NH_3^+$; $B=Pb^{2+}$; and $X=Cl^-$, I^- and/or Br^-)[12-18], excitons are an order of magnitude more weakly bound than in 2D-TMDs [3, 10-11], which made them an excellent platform for a new generation of SCs. Indeed, the conversion efficiency of perovskite-based SCs increased drastically over recent years.[15, 19]

Combining the excellent photostability and the exciton long diffusion length in 2D-TMDs, with the weak exciton binding energy in perovskites into one single hybrid structure may provide a promising new platform for PVs[18, 20-21]. For example, the performance of a tungsten diselenide (WSe_2) monolayer based photodetector was improved by three orders of magnitude following laser healing of the 2D-WSe_2 monolayer and methylammonium lead iodide ($CH_3NH_3PbI_3$) perovskites functionalization[20]. Furthermore, a device made of vertical stacking of 2D materials with $CH_3NH_3PbI_3$ perovskites delivered a high photoresponsivity and photoconductive gains, and after inserting a WSe_2 monolayer within the heterojunction, the device displayed a high on/off ratio transistor behavior[21]. In a heterostructure of $CH_3NH_3PbI_3$ perovskites and a monolayer of molybdenum disulfide (MoS_2), an efficient hole transfer (83%) from perovskites to the MoS_2 monolayer takes place within 320 fs after photoexcitation[18]. In all these studied systems, CT is involved in one way or another. We explore here the ultrafast dynamics of exciton dissociation within a heterostructure composed of a thin layer of $CH_3NH_3PbI_3$ perovskites and a tungsten disulfide (2D-WS_2) monolayer. We employed steady state photoluminescence (PL) and femtosecond pump-probe spectroscopy/microscopy techniques to probe the CT process from the 2D-WS_2 monolayer to perovskites. PL measurements indicated a full quenching of the 2D-WS_2 emission in presence of the perovskites, suggesting that a highly efficient CT took place. In fact, despite carrying out the pump-probe spectroscopy measurements with a temporal resolution of ~45 fs, the CT dynamics were not captured. Based on the energy band alignment of the heterostructure and the ultrafast dynamics of the two lowest excitons of the 2D-WS_2 monolayer, electron transfer was found to be the dominant pathway for exciton dissociation. Furthermore, femtosecond pump-probe measurements indicated that a fraction of the transferred electrons remained in the perovskites up to 2 ns after excitation.

EXPERIMENTAL METHODS

Preparation of 2D-WS_2 monolayers

Monolayers of WS_2 were synthesized on silicon substrates (with a thermally grown 280-nm-thick SiO_2 layer) and sapphire (0001) substrates by chemical vapor deposition. Briefly, WO_3 powder loaded in an alumina crucible was put in the center of the tubular furnace, while sulfur powder was loaded in a separate crucible and put on the upstream. The system was heated up to 800°C in 20 minutes and kept at this temperature for 20 minutes. During the growth, the system was maintained at the atmospheric pressure with a constant argon flow (~30 sccm). After the system was naturally cooled down, the crystals on the substrates were collected for characterizations. To achieve high yield crystals, seeding promoter perylene-3,4,9,10-tetracarboxylic acid tetrapotassium salt (PTAS, 2D Semiconductors USA) was spin-coated on the substrates and dried by nitrogen prior to growth. More details about the material growth and sample transfer were described in our previous report.[22]

Preparation of perovskites

$Pb(OAc)_2{\cdot}3H_2O$ and MAI were purchased from Sigma-Aldrich and used as received. The preparation of $MPbI_3$ film was carried out according to previously reported procedures[23-26]. The $Pb(OAc)_2{\cdot}3H_2O$ (0.8 mmol) and MAI (2.4 mmol) was dissolved in 1 ml of N, N-Dimethylformamide at room temperature. Then the solution was spin-coated onto the substrate containing 2D-WS_2 monolayers at 4000 rpm for 30 seconds. The obtained film was then annealed at 100 C for 10 minutes.

Photoluminescence measurements

The PL spectra were measured using a spectrometer (SP2300, Acton) equipped with a CCD (Pixis 256, Princeton Instruments), coupled to a home built upright-inverted hybrid microscope based on an Olympus IX73. The samples were excited using a second harmonic (400nm) of a Ti:sapphire laser (Coherent, Mira 900) providing pulses centered at 800 nm, 5ps pulses, 76 MHz repetition rate. The repetition rate was reduced to ~ 5 kHz using a pulse picker (Coherent). The output of the pulse picker was frequency doubled using an ultrafast harmonic generator (Coherent 5-050) and directed into a microscope to illuminate the samples through a 100X microscope objective (beam spot ~1 μm). The excitation and emission were carried out on the upright side of the microscope, and consequently, PL was collected on a reflection mode.

Transient absorption spectroscopy/microscopy

A full description of the femtosecond microscope used for pump-probe measurements can be found in previous reports[8, 27]. It is based on a titanium sapphire (Ti:Sa) amplifier (Coherent Legend, USP-HE) seeded by a Ti:Sa oscillator (Micra, Coherent). The amplifier provides pulses centered at 800 nm, with ~45 fs duration and 2.2 W at 1 kHz repetition rate. About 0.5 W is used to generate the pump pulses (3.1 eV) by doubling the 800 nm in a BBO crystal. Another smaller portion (~0.1 W) was used to generate a white light continuum (WLC) probe in a 2-mm thick sapphire window. The WLC covers the spectral range from 450 nm to 900 nm. To minimize temporal chirp, a reflective parabolic mirror was used to collimate the WLC probe. To have a controllable time-delay between the pump and probe, the pump beam was sent through a controllable stage-delay before joining the probe pulse at a dichroic filter (Semrock), which at 45° incidence angle reflects 400 nm and transmits other wavelengths in the visible and near infrared spectrum. The pump and probe beams are then sent collinearly to a reflective objective (36X magnification) to be focused on the sample to ~ 7 μm spot sizes. Noting that since this objective

is reflective, it does not introduce any temporal chirp in the pump and probe beams. The reflected probe is focused onto the entrance slit of a spectrograph (Shamrock 303i, Andor) coupled with a CCD (Newton, Andor) equipped with an electron multiplier (EM). In order to cancel out long-term laser fluctuations, the pump beam passes through an optical chopper set to 500 Hz frequency, allowing the reflection contrast percentage $\Delta R/R_0$ (%) to be calculated between every two successive laser shots. Noting that $\Delta R/R_0$ (%) is calculated as $100\times(R-R_0)/R_0$, with R and R_0 are the intensities of the reflected probe when the pump is on and off, respectively. At each time-delay, 500 $\Delta R/R_0$ (%) were averaged. In order to avoid photo-damaging the sample and many-body interactions, the pump fluence was kept below ~ 2μJ/cm^2 in all pump-probe measurements. The fluence of the pump was maintained the same for all experiments. The instrument response function (IRF) was recorded as in our previous report and suggested a temporal resolution on the order of ~ 45 fs.[27]

RESULTS AND DISCUSSION

Shown in **Figure 1A** is an atomic force microscopy (AFM) image of the studied 2D-WS_2 crystal on a Si/SiO_2 substrate. The height profile of 7 Å indicates that it is a monolayer[27-28]. The steady state absorption spectra of the 2D-WS_2 monolayer on a sapphire substrate and solution of perovskite solution are shown in **Figure 1B**. The perovskites lowest peak is located at ~ 1.6 eV, which is below the 2D-WS_2 lowest band-edge exciton X_A (peak at ~ 2 eV), indicating that dipole-dipole energy transfer from the 2D-WS_2 monolayer to perovskites is possible. In order to predict the CT however, one needs to examine the energy band alignment of the hybrid structure. Based on the values of CB minima (CBMs) and VB maxima (VBMs) previously reported in the literature[18, 28], we constructed a type-I heterojunction for the energy band alignment diagram shown in **Figure 1C**. The 2D-WS_2 lowest band-edge excitons X_A and X_B arise from transitions

between the spin-orbit (SO) split levels CBM1 and CBM2 in the CB and VBM1 and VBM2 in the VB. Since SO split levels in the CB (VB) of the 2D-WS_2 crystal are located at energies higher (lower) than the perovskites CBM (VBM) level, following the photogeneration of excitons in both components of the hybrid upon excitation at 3.1 eV, transfer of both electron and hole from the 2D-WS_2 monolayer to the perovskites are possible. Taking into account the proximity of CBM1 and CBM2[28-30], we note that the transfer driving forces of X_A and X_B electrons are similar. Due to the relatively large SO splitting between VBM1 and VBM2 [28-31], the driving force for the X_B hole transfer is much higher than that of X_A hole.

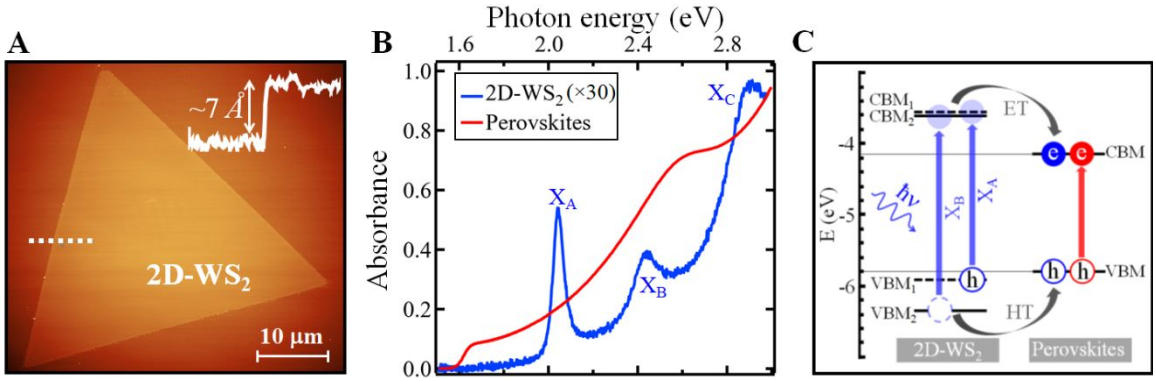

Figure 1. A. AFM image for the studied 2D-WS_2 crystal on a Si/SiO_2 substrate. The inset shows a height profile of 7 Å measured along the dotted line, indicating a single layer thickness. **B.** Steady-state absorption spectra of the perovskites solution in N, N-Dimethylformamide (red plot), and the 2D-WS_2 monolayer on a sapphire substrate (blue plot) magnified 30 times to make the spectral overlap with the absorption spectrum of perovskites visual. The main exciton peaks X_A, X_B, and X_C are indicated. **C.** Band energy alignment of the non-interacting 2D-WS_2 monolayer and the perovskites as reported in the literature[18, 28], outlining the two band-edge excitonic transitions X_A and X_B of the 2D-WS_2 monolayer, which take place between the SO split levels in the VB and CB, and the CBM and VBM energies of the perovskites. Following photoexcitation at 3.1 eV, excitons are generated in both components of the hybrid. Because the perovskites CBM is lower than that of the 2D-WS_2 monolayer, electron transfer (ET) from both X_A and X_B can take place, but because the hole transfer (HT) driving force from VBM2 is greater than that from VBM1, if HT to perovskites takes place, it should be that of X_B exciton.

Energy transfer vs charge transfer

In order to investigate whether charge or energy transfer is the photoinduced process that takes place at the studied hybrid structure, we carried out various PL measurements. Shown in **Figure 2A** is a PL intensity map collected from a sample of a 2D-WS_2 monolayer on a Si/SiO_2 substrate following excitation at 3.1 eV. The intensity was averaged around the emission peak over a range from 1.95 to 2.05 eV. After dispersing a thin layer of perovskites (~ 100 nm thick) on the sample, we collected a new PL intensity map using the same excitation energy and power, but with a different photon-energy average integration range; from 1.5 to 2.05 eV to cover both the perovskites and the 2D-WS_2 monolayer emission peaks. This new PL intensity map shown in **Figure 2B** indicates that on the hybrid area (dark triangle) the PL intensity is quenched. To have more visually quantitative data, shown in **Figure 2C** are PL spectra from the bare 2D-WS_2 crystal, the perovskites, and the hybrid. The PL spectrum measured from the hybrid area shows that while the perovskites emission is quenched by ~ 85%, the 2D-WS_2 emission is fully quenched. Since the 3.1 eV pump is sufficient to excite both; the perovskites and the 2D-WS_2 crystal, excitons are generated in both components of the hybrid. Based on the energy band alignment diagram shown in **Figure 1C**, the quenching of the 2D-WS_2 PL intensity can result from energy, electron, and/or hole transfer to perovskites. If energy transfer to perovskites took place, one expects the perovskites PL intensity to increase, but since it decreased, the pathway of energy transfer from the 2D-WS_2 monolayer to perovskites can be excluded. Noting that energy transfer in the opposite direction is not possible due to the perovskites having a lower band-gap than the 2D-WS_2 monolayer.

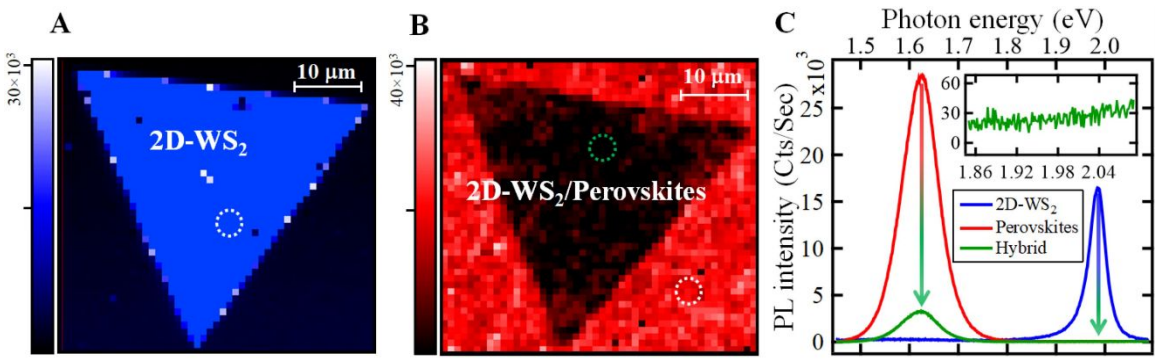

Figure 2. A. PL intensity map of a bare 2D-WS_2 monolayer following excitation at 3.1 eV plotted from the average PL intensity from 1.95 to 2.05 eV. The color bar indicates the intensity in counts/second. The dotted circle indicates the area from which the blue plot in C is taken. **B.** PL intensity map of the 2D-WS_2 monolayer covered with a thin layer of perovskite following excitation at 3.1 eV with the same pump power as in A. The PL intensity was averaged from 1.5 to 2.05 eV. The color bar indicates intensity in counts/second. The dotted circles indicate the areas from which the red and green plots in C are taken. **C.** PL spectra of the bare 2D-WS_2 monolayer (blue plot), perovskites (red plot), and the hybrid (green plot) following excitation at 3.1 eV, indicating PL quenching of both components of the hybrid. The inset is a zoom on the intensity axis around the 2D-WS_2 PL peak from the hybrid sample.

Because the PL intensity was quenched in both components of the hybrid, it is likely that CT took place. Although most reported CT processes from 2D-TMDs were at type II heterojunctions[27, 32-33], CT in a type I heterojunction was reported recently[34]. Following electron (hole) transfer to perovskites from the 2D-WS_2 monolayer, the remaining hole (electron) has no electron (hole) to recombine with and emit a photon from the 2D crystal, which causes quenching of the 2D-WS_2 PL intensity. Because the 2D-WS_2 emission originates from the recombination of electron and hole of X_A exciton rather than from those of X_B exciton, and based on the energy band alignment shown in **Figure 1C**, the driving force for X_A hole transfer is negligible compared to that for X_A electron, the full quenching of the 2D-WS_2 PL is most likely due to electron transfer rather than to hole transfer. We note that hole transfer from higher energy excitons, such as X_B and X_C, is possible. Upon the injection of electrons into the perovskites CB, they occupy some of

the available states in the CB and consequently, the number of newly photogenerated excitons and free charge carriers in the perovskites decreases, thus the number of emitted photons resulting from the radiative recombination of excitons decreases, which explains the quenching in the perovskites PL in the hybrid sample.

To address the concern that the full quenching of the 2D-WS_2 PL observed in the hybrid sample is due to the possibility that the excitation photons do not reach the 2D-WS_2 monolayer and the emitted photons do not reach the detector after depositing the perovskites, we carried out similar experiments but, using a transparent substrate (sapphire), and excited the sample and collected PL from the back side of the transparent substrate. The results shown in **Figure S1** in the *Supporting Information* are similar to those observed in the case of the Si/SiO_2 substrate, which confirms that the PL quenching is indeed due to CT rather than to the perovskites acting as an optical filter for excitation and/or emission.

An approximate estimation of the time-scale of CT based on the PL quenching factor outlined in the *Supporting Information* suggested that CT occurs an fs time-scale. We note that since the quenching in the perovskites and 2D-WS_2 PL intensities in the case of Si/SiO_2 substrate is greater than that in the case of sapphire substrate, the electron transfer time is expected to be shorter than in the case sapphire substrate. This dependence of the CT efficiency on the substrate in heterostructures involving 2D-TMDs is not surprising due to the strong electronic doping induced by CT across the contact interface[9, 35]. For instance, it has been reported that Si/SiO_2 substrate induces more doping to 2D-MoS_2 than $LaAlO_3$ and $SrTiO_3$ substrates[9]. Because electrons are flowing to the monolayer from the Si/SiO_2 substrate, creating a higher electron density, one expects the electron transfer from the 2D-WS_2 crystal to perovskites to be more efficient than in the case of sapphire substrate.

Ultrafast dynamics

In order to get more insights into the CT process at the hybrid structure, we conducted ultrafast pump-probe spectroscopy measurements. A full description of the experimental setup is available in the *Supporting Information* and in our previous reports[8, 27]. The measured quantity as function of photon energy and the time-delay between the pump and probe pulses is $\Delta R/R_0$ (%)$=100\times(R-R_0)/R_0$, where R_0 and R are the intensities of the reflected probe with the pump off and on, respectively.

Shown in **Figures 3A**, **3B**, and **3C** are the pump-probe results obtained from the bare 2D-WS_2 crystal, the perovskites, and the hybrid structure, respectively. Transient spectra cuts at 1, 10, and 50 ps are shown in **Figures 3D**, **3E**, and **3F**, respectively. In the case of the bare 2D-WS_2 monolayer, the transient spectra contain two positive bands around 2 eV and 2.4 eV, corresponding to the depletion of the band-edge excitons X_A and X_B, respectively. When the pump is on, the X_A and X_B excitonic transitions take place, upon the arrival of the probe pulse, the material absorbs less light because the transitions already took place upon the absorption of pump photons, and consequently the intensity of the reflected probe (R) is higher than that in the case when the pump is off (R_0), which makes the transient signal at X_A and X_B photon energies positive. The negative broad bands around 2.2 eV and 2.6 eV correspond to the excited state induced absorption. We note that in a semiconductor, following interband transitions to bring electrons to the CB, these excited electrons can absorb the probe photons to make transitions to even higher energy levels in the CB. Similarly, in the case of the perovskites transient spectra, the negative bands around 1.7 eV and 2.5 eV correspond to the excited state induced absorption. Based on the perovskites steady state absorption spectrum shown in **Figure 1B**, the positive bands around 1.7 eV and 2.45 eV in **Figure 3B** correspond to depleting transitions of excitons and free charge carriers. Although the

low energy band is hidden within the broad negative band, one can tell based on the steady state spectrum of perovskites shown in **Figure 1B**, and on the fact that in transient absorption spectra shown in **Figures 3D**, **3E**, and **3F**, within the excited state induced absorption band around 1.8 eV, there is a peak pointing up corresponding to the depletion of the perovskites lowest exciton. Transient absorption spectra collected from the hybrid structure shown in **Figures 3D**, **3E**, and **3F** contain the features observed in the case of perovskites and the bare 2D-WS_2, but with different amplitudes and dynamics. Because transient spectra from the hybrid sample contained the 2D-WS_2 features, at least the X_A depletion signal, the full quenching of the 2D-WS_2 PL in the hybrid sample, observed in **Figures 2B** and **2C**, is not due to the destruction of the 2D-WS_2 monolayer after depositing the perovskites, but it is due to exciton dissociation.

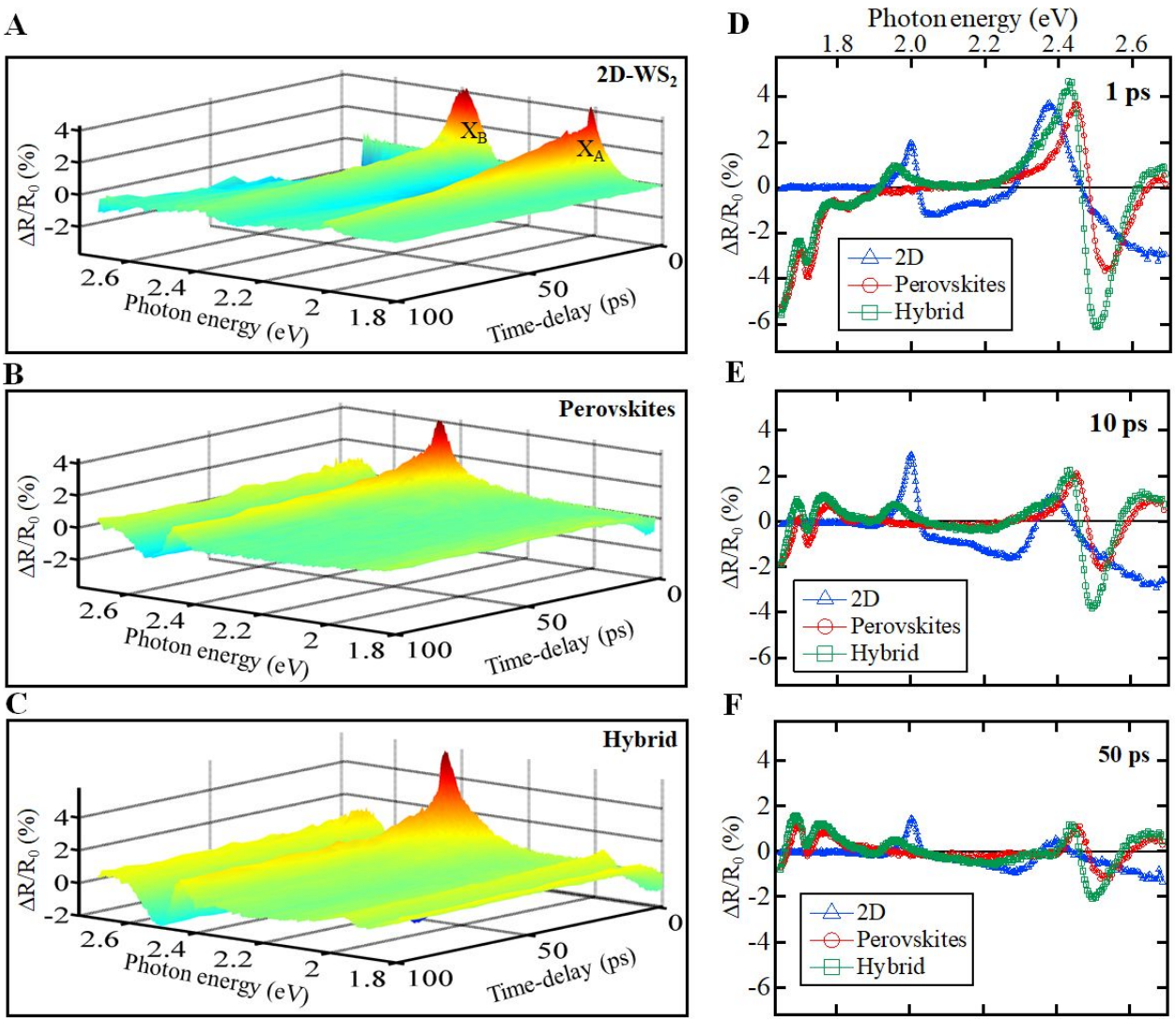

Figure 3. **A.** Transient absorption results following excitation at 3.1 eV. A. Bare 2D-WS_2 monolayer on Si/SiO_2 substrate. **B.** Perovskites on Si/SiO_2 substrat. **C.** Hybrid of 2D-WS_2/Perovskites on Si/SiO_2 substrate. Spectral cuts from **A**, **B**, and **C** as indicated at 1 ps (**D**), at 10 ps (**E**), and at 50 ps (**F**).

In **Figure 4A** we compare the dynamics of perovskites in the bare perovskite sample to those in the hybrid sample, and in **Figure 4B** we compare the dynamics of 2D-WS_2 monolayer in the case of the bare 2D-WS_2 monolayer sample to those in the case of the hybrid sample. Since the perovskites lowest depletion signal (~1.7 eV) is weak and it is hidden by the negative excited state induced absorption (see **Figures 3D**, **3E**, and **3F**), to get more accurate comparison for the

dynamics with and without the 2D-WS_2 monolayer, we plot in **Figure 4A** the dynamics of the higher energy (~2.45 eV) perovskites depletion, which are cuts from **Figure 3B** (bare perovskites area on the sample) and from **Figure 3C** (hybrid area on the sample). For the 2D-WS_2 monolayer, we plot in **Figure 4B** the dynamics of exciton X_A for the bare 2D-WS_2 crystal (cut at 2 eV from **Figure 3A**) and those from the hybrid sample (cut at 2 eV from **Figure 3C**). These dynamics are fit with multi-exponential decay functions and the fit parameters are listed in **TABLE 1**.

When charges are transferred to perovskites from the 2D-WS_2 monolayer, one expects to observe depletion of the perovskite ground state peaks, which according to the steady state absorption spectrum shown in **Figure 1B**, are located at ~1.7 and 2.45 eV. Because some of the perovskites ground state population is already depleted due to direct excitation by the pump, an increase in the amplitude of the depletion signal in the case of the hybrid sample would indicate that electron, hole or energy transfer from the 2D-WS_2 crystal to the perovskites took place. But because the pathway of energy transfer was eliminated based on PL results, we will limit the discussion to CT. Since the hybrid sample was excited with the same pump energy and fluence, one expects to generate the same number of excitons and free charge carriers in the perovskites, and consequently the percentage of depleted population should be the same as in the case of the bare perovskites sample (~2.5%), but according to **Figure 4A**, the signal amplitude in the case of the hybrid sample is doubled (~5%). The additional ~2.5% population depletion is due to CT from the 2D-WS_2 monolayer. We note that the perovskites film is on top of the 2D-WS_2 monolayer, facing the incident laser beams, therefore, the number of pump photons reaching the perovskite is the same in both cases of hybrid and bare perovskite samples.

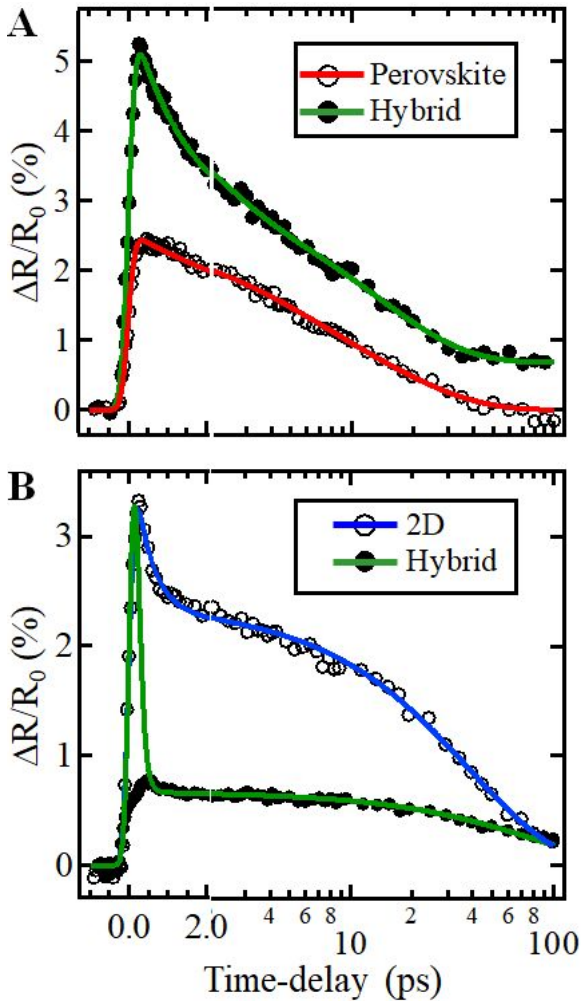

Figure 4. A. Dynamics of the perovskites depletion in the absence (open circles) and presence (filled circles) of the 2D-WS_2 monolayer. Solid plots are fits to a multiexponential decay function convoluted with a 45 fs short Gaussian excitation pulse. **B.** Dynamics of the 2D-WS_2 exciton X_A depletion signal in the case of the bare 2D-WS_2 monolayer (open circle) and hybrid sample (filled circles), fit to a bi-exponential decay function convoluted with a 45 fs short Gaussian excitation pulse (solid line plots). In the case of the hybrid sample, the fit is forced to have the initial amplitude equal to that in the case of the bare 2D-WS_2 sample because since the pump energy and fluence are similar in both experiments, the number of photogenerated excitons should be comparable. The time-delay axes are shown in a linear scale up to 2 ps, and logarithmic scale thereafter.

To address whether or not the transferred charges remained in the perovskites, at least up to the time-scale examined here (100 ps), we consider the dynamics of the perovskites depletion signal shown in **Figure 4A**. We note that because of the spectral shifts, in the case of the bare

perovskite sample we average the dynamics from 2.40 to 2.47 eV and in the case of the hybrid sample the dynamics are averaged from 2.37 to 2.44 eV. In the absence of the 2D-WS_2 monolayer, a bi-exponential decay function described well the perovskites depletion recovery dynamics, and the fit parameters are listed in **TABLE 1**. About 36% of the population decays with a time-constant of ~ 4 ps, and the remaining population decays with a time-constant of 16 ps. One can see visually from **Figure 4A** that by about 50 ps time-delay, the perovskites depletion signal completely recovered. In the case of the hybrid sample however, although we attempted to fit the dynamics using only two exponential components similar to the case of bare perovskites sample, the converged fit missed the dynamics at later time-delays, and required a third exponential decay component to describe traces at later time-delays. The first two components were comparable to those obtained in the case of the bare perovskites sample, but about ~12% of the depleted population recovers with a time-constant of ~ 2.2 ns, indicating that some of the transferred charges are still in the perovskites up to ~ 2 ns. This is three orders of magnitude longer than in the case of 2D-WS_2/quantum dot (QD) heterostructure, where the transferred electrons from the 2D-WS_2 monolayer to a single layer of cadmium selenide (CdSe) QDs recombine with the hole left in the 2D-WS_2 monolayer within a ps time-scale.[27]

TABLE 1: List of the fit parameters of the perovskite's exciton depletion recovery dynamics in the presence and absence of the 2D-WS_2 monolayer, and the 2D-WS_2 exciton X_A depletion recovery dynamics for the bare 2D-WS_2 monolayer and the hybrid samples. A_i and t_i are the amplitude and time constant of the exponential component i.

	Perovskites exciton		2D-WS_2 exciton X_A	
	Perovskite	Hybrid	2D	Hybrid
A_1 (%)	36	45	41	94
t_1 (ps)	4.2	1.4	0.43	0.09
A_2 (%)	64	43	59	6
t_2 (ps)	16.2	13.7	38.9	79
A_3 (%)		12		

t_3 (ps) 2200

For the dynamics of the 2D-WS_2 exciton X_A, because in the case of the hybrid sample the depletion peak shifted to the "red" by ~ 40 meV compared to the bare 2D-WS_2 sample (see **Figure S2** in the *Supporting Information*) we plot in **Figure 4B** the dynamics of X_A exciton averaged around the depletion peak from 1.96 eV to 2.03 eV and from 1.93 eV to 1.99 eV for the bare 2D-WS_2 and the hybrid samples, respectively.

In the case of the bare 2D-WS_2 sample, about 40% of the excited population decays with a time constant of ~430 fs, and the remaining population decays with a time constant of ~40 ps. The observation of slow and fast effective decay components was previously reported for different 2D-TMD monolayers[28, 36-39]. Although assigning each decay component to radiative or non-radiative processes is not trivial, a few groups have reported on this assignment. For instance, in the case of 2D-MoS_2 monolayers, temperature and the pump fluence dependent measurements suggested that exciton dynamics are dominated on the sub-ps time-scale by thermalization and relaxation and thereafter by defect assisted recombination[37]. In the case of the hybrid sample, the signal amplitude (the percentage of depleted population) is three times less than that in the case of the bare 2D-WS_2 sample. Based on the previous discussion regarding the dynamics of the perovskites depletion signal, which indicated that CT from the 2D-WS_2 monolayer took place at early time-delays (shorter than the temporal resolution of the experiment), one can attribute the ~70% *missing* population of the 2D-WS_2 exciton X_A at the hybrid sample at early time-delays to CT to perovskites. Although the perovskite's film in the hybrid sample is about 10^5 times thinner than the cuvette (1 cm thick) used to measure the steady-state absorption spectrum (shown in **Figure 1B**) of the perovskite's solution, the 2D-WS_2 monolayer can be influenced by the interference from the presence of the perovskite's layer. But, because the measured imaginary dielectric

constant of the 2D-WS_2 monolayer (~22)[40] is almost seven times that of the perovskites (~3.5)[41], the screening of the Coulomb potential effects is less efficient[42]. Under these circumstances, we can consider that the initial number of photo-generated excitons in the hybrid sample is comparable to that in the bare 2D-WS_2 sample. To account for the ~70% *missing* population of the 2D-WS_2 exciton X_A in the hybrid sample at early time-delays, we forced the fit (green plot in **Figure 4B**) to consider the initial amplitude equal to that in the case of the bare 2D-WS_2 monolayer sample (because the number of generated excitons is comparable in both samples), and run the fit. Although the fit at later time-delays describes the data and thus provides a meaningful time-constant, at early time-delays it is not the case because there are no data points (due to electron transfer happening faster than the temporal resolution), but it visually informs the reader that at early time-delays there is an uncaptured ultrafast decay due to CT.

Electron transfer vs. Hole transfer

Based on the energy diagram shown in **Figure 1C**, the driving forces for electron transfer from X_A and X_B excitons to the perovskite are similar. However, for hole transfer from the 2D-WS_2 monolayer to perovskites, although the hole of X_B has a higher driving force to transfer to perovskites because it is located at VBM2, which is more than 400 meV below the perovskite's VBM, the hole of X_A still can transfer to perovskites through tunneling due to resonance between VBM1 and the perovskite's VBM. Taking into consideration the large thickness of the perovskite's film (~100 nm) compared to that of the 2D-WS_2 monolayer (< 1 nm), the transferred hole needs extra kinetic energy above that needed for crossing the barrier. Furthermore, it has been reported recently that due to the strong exciton binding energy in 2D-WS_2 monolayers, a *horizontal* hole transfer through tunneling is unlikely to happen[42]. Consequently, the hole of X_B is likely to transfer to perovskites more efficiently than the hole of X_A exciton. In the pump-probe

measurements, this will manifest as a strong decay of exciton X_B depletion signal in the case of the hybrid sample. Thus, to estimate whether electron or hole transfer is the dominant pathway of CT, one needs to compare the decay of X_A exciton depletion (which is caused by electron transfer) to the decay of X_B exciton depletion (which is caused by both electron and hole transfers). This comparison, outlined in **Figure S3** and corresponding text in the *Supporting Information*, suggests that at early time-delays (<1 ps) unlike in the case of X_A exciton where the depletion signal amplitude decreased by ~ 70% (due to electron transfer), the percentage of X_B depleted population decreased by only ~30%. If the efficiency of hole transfer was comparable to that of electron transfer, the decrease in the amplitude of X_B depletion signal at the hybrid sample should be at least ~70% as well. In conclusion, the electron transfer efficiency is at least more than twice greater than that of hole transfer.

CONCLUSION

In summary, the full quenching of the 2D-WS_2 monolayer PL after loading the perovskites thin layer on the sample suggested that either CT or energy transfer to perovskites took place in the hybrid. Because the perovskites PL intensity decreased, the energy transfer hypothesis was ruled out. Based on the band energy alignment of the heterostructure, we attributed the quenching of the 2D-WS_2 PL to CT. An estimation of the CT time based on the 2D-WS_2 PL quenching factor suggested that the transfer occurs on a fs time-scale. Pump-probe measurements confirmed that CT to perovskites took place based on two main observations at the hybrid sample: 1) the amplitude of the perovskites depletion signal was doubled compared to the case of bare perovskites sample, and 2) the amplitudes of X_A and X_B exciton depletion signals of the 2D-WS_2 monolayer decreased by ~70% and ~30%, respectively compared to the case of bare 2D-WS_2 sample. Because at the hybrid sample the decrease in X_A depletion signal was more than twice that of X_B,

we concluded that electron transfer is likely the dominant pathway of CT. Additionally, these measurements suggested that a fraction of the transferred electrons remained in the perovskites up to ~2 ns after the transfer.

Supporting Information

Figure S1 for photoluminescence measurements using a transparent substrate, Figure S2 outlining the shift of exciton depletion at the hybrid sample, and Figure S3 comparing the dynamics of X_A and X_B excitons. Table S1 listing the parameters of the converged fits of X_B exciton dynamics. An estimation of the charge transfer time based on the charge donor's PL quenching factor.

ACKNOWLEDGMENTS

This research was conducted at the Center for Nanophase Materials Sciences, which is a DOE Office of Science User Facility. Synthesis of the two-dimensional materials was supported by the Materials Science and Engineering Division, Office of Basic Energy Sciences, U.S. Department of Energy. J. B., L. Q., and A. B. acknowledge support by the CSUN College of Science and Math new Faculty Startup Funds, Research & Graduate Studies Office, and Associated Students for sponsoring the travel to ORNL.

REFERENCES

(1) O'Regan, B.; Grätzel, M. A low-cost, high-efficiency solar cell based on dye-sensitized colloidal TiO_2 films. *Nature* **1991,** *353*, 737-740.

(2) Hagfeldt, A.; Boschloo, G.; Sun, L.; Kloo, L.; Pettersson, H. Dye-Sensitized Solar Cells. *Chem. Rev.* **2010,** *110*, 6595-6663.

(3) Miyata, A.; Mitioglu, A.; Plochocka, P.; Portuga, O.; Wang, J. T.-W.; Stranks, S. D.; Snaith, H. J.; Nicholas, R. J. Direct measurement of the exciton binding energy and ective masses for charge carriers in organic–inorganic tri-halide perovskites. *Nat. Phys.* **2015,** *11*, 582-588.

(4) Tsai, M.-L.; Su, S.-H.; Chang, J.-K.; Tsai, D.-S.; Chen, C.-H.; Wu, C.-I.; Li, L.-J.; Chen, L.-J.; He, J.-H. Monolayer MoS_2 Heterojunction Solar Cells. *ACS Nano* **2014,** *8*, 8317–8322.

(5) Gan; L.-Y.; Zhang, Q.; Cheng, Y.; Schwingenschlögl, U. Photovoltaic Heterojunctions of Fullerenes with MoS_2 and WS_2 Monolayers. *J. Phys. Chem. Lett.* **2014,** *5*, 1445–1449.

(6) Bernardi, M.; Palummo, M.; Grossman, J. C. Extraordinary Sunlight Absorption and One Nanometer Thick Photovoltaics Using Two-Dimensional Monolayer Materials. *Nano Lett.* **2013,** *13*, 3664–3670.

(7) He, J.; He, D.; Wang, Y.; Cui, Q.; Ceballosb, F.; Zhao, H. Spatiotemporal dynamics of excitons in monolayer and bulk WS_2. *Nanoscale* **2015,** *7*, 9526-9531.

(8) Boulesbaa, A.; Babicheva, V. E.; Wang, K.; Kravchenko, I. I.; Lin, M.-W.; Mahjouri-Samani, M.; Jacobs, C. B.; Puretzky, A. A.; Xiao, K.; Ivanov, I.; et al. Ultrafast Dynamics of Metal Plasmons Induced by 2D Semiconductor Excitons in Hybrid Nanostructure Arrays. *ACS Photonics* **2016,** *3*, 2389–2395.

(9) Li, Y.; Qi, Z.; Liu, M.; Wang, Y.; Cheng, X.; Zhang, G.; Sheng, L. Photoluminescence of monolayer MoS_2 on $LaAlO_3$ and $SrTiO_3$ substrates. *Nanoscale* **2014,** *6*, 15248-15254.

(10) He, K.; Kumar, N.; Zhao, L.; Wang, Z.; Mak, K. F.; Zhao, H.; Shan, J. Tightly Bound Excitons in Monolayer WSe_2. *Phys. Rev. Lett.* **2014,** *113*, 026803.

(11) Kidd, D. W.; Zhang, D. K.; Varga, K. Binding energies and structures of two-dimensional excitonic complexes in transition metal dichalcogenides. *Phys. Rev. B* **2016,** *93*, 125423.

(12) Im, J.;-H.; Lee, C.-R.; Lee, J.-W.; Park, S.-W.; Park, N.-G. 6.5% efficient perovskite quantum-dot-sensitized solar cell. *Nanoscale* **2011,** *3*, 4088-4093.

(13) Lee, M. M.; Teuscher, J.; Miyasaka, T.; Murakami, T. N.; Snaith, H. J. Efficient Hybrid Solar Cells Based on Meso-Superstructured Organometal Halide Perovskites. *Science* **2012,** *338*, 643-647.

(14) Kojima, A.; Teshima, K.; Shirai, Y.; Miyasaka, T. Organometal Halide Perovskites as Visible-Light Sensitizers for Photovoltaic Cells. *J. Am. Chem. Soc.* **2009,** *131*, 6050-6051.

(15) Green, M. A.; Ho-Baillie, A; Snaith, H. J. The emergence of perovskite solar cells. *Nat. Photonics* **2014,** *8*, 506-514.

(16) Kim, H.-S.; Lee, J.-W.; Yantara, N.; Boix, P. P.; Kulkarni, S. A.; Mhaisalkar, S.; Grätzel, M.; Park, N.-G. High Efficiency Solid-State Sensitized Solar Cell-Based on Submicrometer Rutile TiO_2 Nanorod and $CH_3NH_3PbI_3$ Perovskite Sensitizer. *Nano Lett.* **2013,** *13*, 2412-2417.

(17) Yang, B.; Dyck, O.; Poplawsky, J.; Keum, J.; Puretzky, A.; Das, S.; Ivanov, I.; Rouleau, C.; Duscher, G.; Geohegan, D.; et al. Perovskite Solar Cells with Near 100% Internal Quantum Efficiency Based on Large Single Crystalline Grains and Vertical Bulk Heterojunctions. *J. Am. Chem. Soc.* **2015,** *137*, 9210–9213.

(18) Peng, B.; Yu, G.; Zhao, Y.; Xu, Q.; Tan, R. S.; Tang, W.; Lu, H.; Xie, J.; Deng, L.; Sum, T. C.; et al. Achieving Ultrafast Hole Transfer at the Monolayer MoS_2 and $CH_3NH_3PbI_3$ Perovskite Interface by Defect Engineering. *ACS Nano* **2016,** *10*, 6383-6391.

(19) Yang, S.; Fu, W.; Zhang, Z.; Chen, H.; Li, C.-Z. Recent advances in perovskite solar cells: efficiency, stability and lead-free perovskite". *J. Mater. Chem. A* **2017,** *5*, 11462-11482.

(20) Lu, J.; Carvalho, A.; Liu, H.; Lim, S. X.; Castro Neto, A. H.; Sow, C. H. Hybrid Bilayer WSe_2–$CH_3NH_3PbI_3$ Organolead Halide Perovskite as a High-Performance Photodetector. *Angew. Chem.* **2016,** *128*, 12124-12128.

(21) Cheng, H.-C.; Wang; G.; Li, D.; He, Q.; Yin, A.; Liu, Y.; Wu, H.; Ding, M.; Huang, Y.; Duan, X. van der Waals Heterojunction Devices Based on Organohalide Perovskites and Two-Dimensional Materials. *Nano Lett.* **2016,** *16*, 367-373.

(22) Wang, K.; Huang, B.; Tian, M.; Ceballos, F.; Lin, M.-W.; Mahjouri-Samani, M.; Boulesbaa, A.; Puretzky, A. A.; Rouleau, C. M.; Yoon; M.; et al. Interlayer Coupling in Twisted WSe_2/WS_2 Bilayer Heterostructures Revealed by Optical Spectroscopy. *ACS Nano* **2016,** *10*, 6612–6622.

(23) Zhang, W.; Saliba, M.; Moore, D. T.; Pathak, S. K.; Hörantner, M. T.; Stergiopoulos, T.; Stranks, S. D.; Eperon, G. E.; Alexander-Webber, J. A.; Abate, A.; et al. Ultrasmooth organic–inorganic perovskite thin-film formation and crystallization for efficient planar heterojunction solar cells. *Nat. Commun.* **2015,** *6*, 6142.

(24) Zhao, L.; Luo, D.; Wu, J.; Hu, Q.; Zhang, W.; Chen, K.; Liu, T.; Liu, Y.; Zhang, Y.; Liu, F.; et al. High‐Performance Inverted Planar Heterojunction Perovskite Solar Cells Based on Lead Acetate Precursor with Efficiency Exceeding 18%. *Adv. Funct. Mater.* **2016,** *26*, 3508-3514.

(25) Qiu, W.; Merckx, T.; Jaysankar, M.; Masse de la Huerta, C.; Rakocevic, L.; Zhang, W.; Paetzold, U. W.; Gehlhaar, R.; Froyen, L.; Poortmans, J.; et al. Pinhole-free perovskite films for efficient solar modules. *Energy Environ. Sci.* **2016,** *9*, 484-489.

(26) Qing, J.; Chandran, H.-T.; Cheng, Y.-H.; Liu, X.-K.; Li, H.-W.; Tsang, S.-W.; Lo, M.-F.; Lee, C.-S.; Chlorine Incorporation for Enhanced Performance of Planar Perovskite Solar Cell Based on Lead Acetate Precursor. *ACS Appl. Mater. Interfaces* **2015,** *7*, 23110-23116.

(27) Boulesbaa, A.; Wang, K.; Mahjouri-Samani, M.; Tian, M.; Puretzky, A. A.; Ivanov, I.; Rouleau, C.; M.; Xiao, K.; Sumpter, B. G.; Geohegan, D. B. Ultrafast Charge Transfer and Hybrid Exciton Formation in 2D/0D Heterostructures. *J. Am. Chem. Soc.* **2016,** *138*, 14713-14719.

(28) Boulesbaa, A.; Huang, B.; Wang, K.; Lin, M.-W.; Mahjouri-Samani, M.; Rouleau, C.; Xiao, K.; Yoon, M.; Sumpter, B.; Puretzky, A.; et al. Observation of two distinct negative trions in tungsten disulfide monolayers. *Phys. Rev. B* **2015,** *92*, 115443.

(29) Mai, C.; Semenov, Y. G.; Barrette, A.; Yu, Y.; Jin, Z.; Cao, L.; Kim, K. W.; Gundogdu, K. Exciton valley relaxation in a single layer of WS_2 measured by ultrafast pectroscopy. *Phys. Rev. B* **2014,** *90*, 041414(R).

(30) Kośmider, K.; González, J. W.; Fernández-Rossier, J. Large spinsplitting in the conductionbandof transition metaldichalcogenidemonolayers. *Phys. Rev. B* **2013,** *88*, 245436

(31) Kang, J.; Tongay, S.; Zhou, J.; Li, J.; Wu, J. Band offsets and heterostructures of two-dimensional semiconductors. *Appl. Phys. Lett.* **2013,** *102*, 012111.

(32) Hong, X.; Kim, J.; Shi, S.-F.; Zhang, Y.; Jin, C.; Sun, Y.; Tongay, S.; Wu, J.; Zhang, Y.; Wang, F. Ultrafast charge transfer in atomically thin MoS_2/WS_2 heterostructures. *Nat. Nanotechnol.* **2014,** *9*, 682-686.

(33) Chen, H.; Wen, X.; Zhang, J.; Wu, T.; Gong, Y.; Zhang, X.; Yuan, J.; Yi, C.; Lou, J.; Ajayan, P. M.; et al. Ultrafast formation of interlayer hot excitons in atomically thin MoS_2/WS_2 heterostructures. *Nat. Commun.* **2016,** *7*, 12512.

(34) Bellus, M. Z.; Li, M.; Lane, S. D.; Ceballos, F.; Cui, Q.; Cheng Zeng, X.; Zhao, H. Type-I van der Waals heterostructure formed by MoS_2 and ReS_2 monolayers. *Nanoscale Horiz.* **2017,** *2*, 31-36.

(35) Buscema, M.; Steele, G. A.; van der Zant, H. S. J.; Castellanos-Gomez, A. The effect of the substrate on the Raman and photoluminescence emission of single-layer MoS_2. *Nano Res.* **2014,** *7*, 561-571.

(36) Shi, H.; Yan, R.; Bertolazzi, S.; Brivio, J.; Gao, B.; Kis, A.; Jena, D.; Xing, H. G.; Huang, L. Exciton Dynamics in Suspended Monolayer and Few-Layer MoS_2 2D Crystals. *ACS Nano* **2013,** *7* (2), 1072-1080.

(37) Wang, H.; Zhang, C.; Rana, F., Ultrafast Dynamics of Defect-Assisted Electron−Hole Recombination in Monolayer MoS_2. *Nano Lett.* **2015,** *15*, 339-345.

(38) Moody, G.; Schaibley, J.; Xu, X. Exciton dynamics in monolayer transition metal dichalcogenides. *J. Opt. Soc. Am. B* **2016,** *33*, C39-C49.

(39) Cui, Q.; Ceballos, F.; Kumar, N.; Zhao, H. Transient Absorption Microscopy of Monolayer and Bulk WSe_2. *ACS Nano* **2014,** *8*, 2970-2976.

(40) Li, Y.; Chernikov, A.; Zhang, X.; Rigosi, A.; Hill, H. M.; van der Zande, A. M.; Chenet; D. A.; Shih, E.-M.; Hone, J.; Heinz, T. F. Measurement of the optical dielectric function of monolayer transition-metal dichalcogenides: MoS_2, $MoSe_2$, WS_2, andWSe_2. *Phys. Rev. B* **2014,** *90*, 205422.

(41) Wang, Z.; Yuan, S.; Li, D.; Jin, F.; Zhang, R.; Zhan, Y.; Lu, M.; Wang, S.; Zheng, Y.; Guo, J.; Fan, Z.; Chen, L. Influence of hydration water on $CH_3NH_3PbI_3$ perovskite films prepared through one-step procedure. *Opt. Express* **2016,** *24* (22), A1431-A1443.

(42) Zhu, T.; Yuan, L.; Zhao; Y.; Zhou, M.; Wan, Y.; Mei, J.; Huang, L. Highly mobile charge-transfer excitons in two-dimensional WS_2/tetracene heterostructures. *Sci. Adv.* **2018,** *4*, eaao3104.
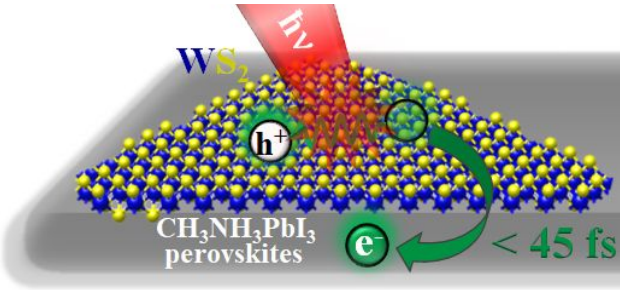
TOC Graphic